Exploiting Bird Locomotion Kinematics Data for Robotics Modeling

Vincent Hugel – corresponding author
Engineering System Laboratory, University of Versailles,
10/12 avenue de l'Europe, 78140 VÉLIZY, France
Email: hugel@lisv.uvsq.fr
Rémi Hackert, and Anick Abourachid
Muséum National d'Histoire Naturelle de Paris (MNHN),
55 rue Buffon, 75005 PARIS, France,
E-mail: Remi.Hackert@animals-in-motion.com, abourach@mnhn.fr

***Abstract*—We present here the results of an analysis carried out by biologists and roboticists with the aim of modeling bird locomotion kinematics for robotics purposes. The aim was to develop a bio-inspired kinematic model of the bird leg from biological data. We first acquired and processed kinematic data for sagittal and top views obtained by X-ray radiography of quails walking. Data processing involved filtering and specific data reconstruction in three dimensions, as two-dimensional views cannot be synchronized. We then designed a robotic model of a bird-like leg based on a kinematic analysis of the biological data. Angular velocity vectors were calculated to define the number of degrees of freedom (DOF) at each joint and the orientation of the rotation axes.**

***Index Terms*—bird leg kinematics, robotics modeling**

Exploiting Bird Locomotion Kinematics Data for Robotics Modeling

I. Introduction

TWO bipeds have succeeded in colonizing the Earth: birds and humans. Most robotics projects have used humans as the model of biped robot design [1]–[5]. One of the reasons for this is that robots resembling humans may appear less threatening, encouraging people to trust the machine and to interact with it. We also know more about the structure of humans, as many studies of human locomotion have been carried out. We know far less about birds than about humans, but this does not necessarily mean that they are worse mechanical models.

Birds are found in every kind of environment, worldwide [6], [7]. All birds have the same basic leg structure, although variation is observed in the length of the segments. Whereas humans walk on their whole foot, birds walk on their toes. The human foot contains a large number of bones, whereas the bird foot is divided into two parts: a long segment and the toes - generally with three toes pointing forwards and a smaller toe pointing backwards. The bird leg consists of three long segments and four joints, whereas the human leg has two segments and three joints. The simple structure of the bird foot can serve as the inspiration for a robotic foot. The structures of the human and bird legs are shown in Figure 1, with the names of the different segments and joints indicated.

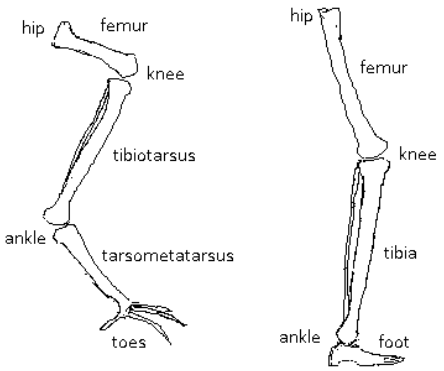

Fig. 1. Comparison of the legs of birds and humans

The terrestrial locomotion system of birds includes several interesting mechanical features. First, the center of mass is located under the hip, near the knee. This low center of gravity should confer a higher level of stability. Second, the four joints and their flexed position provide redundancy in mobility, providing greater stability on uneven ground [8]. Third, the ratio between stride length and hip height is about 2.2 for quails, whereas it is about 1 for human beings. Quails are thus able to take very large strides. Thanks to these features, the bird leg locomotor apparatus may be a useful alternative to designs based on the human leg for the design of robots.

Very few biological studies of bird locomotion based on three-dimensional(3D) kinematic data have been carried out. Indeed, it is difficult to use 3D motion analysis systems, such as the six-camera VICON system, on birds because the body and most of the legs are covered with feathers, ostriches constituting a notable exception as they have very few feathers on their legs. The VICON motion analysis system usually used in analyses of human motion can be applied to ostriches [9]. The motion of small birds can be studied by using X-ray data to follow the motion of the bones. This approach is not often used, and is generally restricted to the lateral motion component, because the X-ray machine has only one transmitter and generates one X-ray beam at a time. Most published results have therefore been derived from two-dimensional (2D) data [10]–[13]. As the motion of bird legs is really three-dimensional, we need to obtain 3D data if we are to understand motion fully, even in small birds. Our principal aim was to develop a technique for reconstructing 3D motion data from 2D views of quails walking through an X-ray beam. We used sagittal and the dorso-ventral (DV) 2D views, which were not synchronized because the direction of the X-ray beam had to be changed between lateral and DV recordings.

Very few 3D kinematic modeling studies of walking birds have been carried out. One study on ostriches led to the design of a kinematic model based on anatomical data that was then used as a reference for the reconstruction of ostrich bone motion from data for the motion of anatomic landmark recorded with the VICON system whilst the animals were running [9]. Biological 3D reconstruction has also been achieved using inverse kinematics solutions under constraints, to validate plausible modes of bipedal locomotion for extinct humanoid species [14]. We worked from direct recordings of motion and made use of the reconstructed 3D data to define a kinematic model of terrestrial bird locomotion. This model will then be used in the design of a robotics model.

Most research into biped robots has focused on anthropomorphic robots. Very few robots have been developed from kinematic models inspired from the bird locomotor apparatus. One such robot, the Meltran II robot, was designed in the framework of the MELTRAN project of MEL[1]. This robot was a planar prototype with six active DOF. It was equipped with only two segments per leg. It was one of the first non anthropomorphic robots to be produced that could walk both forwards and backwards. The main difference between this robot and human-like robots is that its knee joint points backwards rather than forwards. This robot was designed to implement dynamic control laws [15], based on a linearized

[1]Mechanical Engineering Laboratory, Tsukuba, Japan

Fig. 2. Quail walking on treadmill

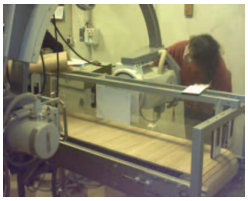

Fig. 3. X-Ray cineradiography system

inverted pendulum, assuming that the legs have no mass. Other researchers from MIT have built bipeds resembling birds - the Spring-Turkey and Spring-Flamingo robots [16] [17]. These robots are also constrained in the sagittal plane and have serial elastic actuators to favor the natural dynamics of robot limbs rather than actuator dynamics. MIT researchers have also designed and built a two-legged dinosaur-like robot called Troody [18], equipped with 16 electric motors in the hips, knees, ankles, feet, and tail. However, little information was been published concerning the kinematic design of its 3D leg structure. These robots may have legs physically resembling those of birds or dinosaurs, but their kinematics did not result from a biological study because they were developed for different reasons: for the application of control laws, displacement autonomy and so on.

We describe here an experimental protocol used to collect kinematic data for walking quails and the techniques used to reconstruct the data in three dimensions. The reconstructed data were then used to analyze bird leg kinematics in three dimensions, for the inference of a bio-inspired kinematic model. Angular velocity vectors were calculated to define the number of degrees of freedom (DOF) at each joint and the orientation of the rotation axes.

II. BIOLOGICAL EXPERIMENTS AND ANALYSIS

A. Experimental setup and data acquisition

Six quails (*Coturnix coturnix japonica*) were filmed walking on a trail in an X-ray beam (fig. 2). The beam was first made horizontal to record the lateral projection of the moving skeleton, using a 250 Hz video-camera system coupled to the X-ray cineradiography device (fig. 3). The machine was then moved such that the X-ray beam was vertical, to capture the dorso-ventral projection of the moving skeleton. We stuck small lead balls to points on the vertebral column (VC) and close to the leg joints - VC anterior point (VC_a) and VC posterior point (VC_p), hip joint (H), knee joint (K), ankle joint (A) and foot joint (F) - to ensure that exactly the same points were followed on the two projections. Toe and head points were also followed but are not analyzed here. Figure 4 shows an X-ray image in sagittal view and another in top view. The 2D coordinates of the lead balls were extracted from X-ray video images in a semi-automated system based on the tracking of balls with algorithms implemented in Matlab. These image processing algorithms were based on cross-correlation procedures using a reference black disk of the same size as the lead balls. In this system, it is possible for the user to stop the tracking procedure and correct the position

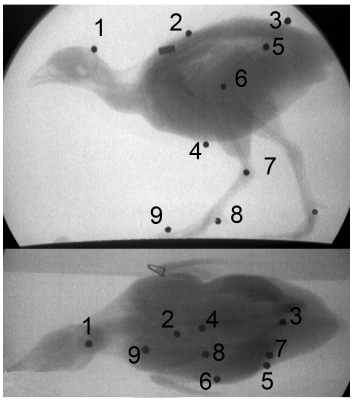

Fig. 4. Parasagittal view and top view X-ray images. 1. Head. 2. VC anterior point. 3. VC posterior point. 4. Sternum keel. 5. Hip. 6. Knee. 7. Ankle. 8. Foot. 9. Toe.

of the exploration window in the image if necessary. Below, the x direction is the longitudinal direction of motion. The y direction denotes the horizontal, lateral axis. The z direction is the vertical direction. The sagittal view gives (x, z) coordinates and the DV view gives (x, y) coordinates.

B. 3D reconstruction from non-synchronized 2D views

The 3D reconstruction technique proposed here is not based on the *motion warping* method used by some biologists [19] [20] to correct trajectories. The *motion warping* method makes local adjustments to trajectories based on space-time constraints or criteria relating to biomechanical laws. This method may simultaneously change the shape of the stride phase and the swing phase. By contrast, our method considers these two phases separately, so as to reflect independent variations in the length of the stride and swing phases, as observed in real situations when the animal walks at different speeds. The duration of the swing phase is actually almost constant, whereas the duration of the stance phase decreases with increasing speed [21]. The 3D reconstruction technique described here aims to match walking cycles in 2D lateral and DV views, using the longitudinal foot coordinate, x_{foot}. This coordinate is obtained in both views. A walking cycle is defined as the period between two consecutive footfalls for the same foot. The method can be broken down into the following steps:

1) **Filtering**. All x, y and z signals for the foot, ankle, knee, hip, anterior point of the VC, posterior point of the VC and sternum keel were filtered using a Butterworth low-pass filter. The sampling frequency F_e of signals was 250 Hz and the filter cut-off frequency F_c was $20\,Hz$ ($F_c/F_e = 0.08$). The cut-off frequency was determined from the frequency spectrum of the signal. The Butterworth filter is a fifth-order IIR filter (infinite impulse response) that keeps the amplitude constant for signal components below the cut-off frequency. However, it introduces a fixed phase shift. This phase shift can be removed by applying the filter to the signal, reversing the resulting signal in terms of time, re-applying the filter and reversing the signal in terms of time again.

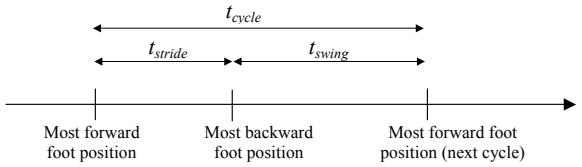

Fig. 5. Definition of cycle, swing and stride periods relative to x longitudinal foot position.

The start and end of the filtered signal are removed to prevent divergence.

2) **Calculating averages for the swing and cycle periods in lateral and DV views**. The swing time is defined as the time interval between the furthest back x position of the foot in the current cycle and the furthest forward x position in the next cycle (protraction). The cycle time is defined as the time interval between two successive foot furthest forward x positions. It is the sum of the swing and stride times (fig. 5 and 9). The stride time is defined as the time interval between the furthest backward and furthest forward x positions in a given step cycle (retraction). For each lateral and DV recording, the mean swing period $< t_{swing} >$ and the mean cycle period $< t_{cycle} >$ were calculated for all valid cycles.
3) **Selecting the best matching lateral and DV views**. For each lateral view, the best matching DV view is that for which the mean swing period is closest to the mean swing period for the lateral view concerned. These lateral and DV views are called matching views.
4) **Calculating mean swing period and mean cycle period for matching views**. In this step, we calculated the mean swing period and the mean cycle period extracted from the two matching views.
5) **Extracting valid cycles from the foot signal** x_{foot}. The algorithm obtains continuous foot cycles by extracting portions of signal delimited by successive times at which x_{foot} is 0 - i.e. at which the foot enters the same transverse plane as the anterior VC point.
6) **Scaling up/down extracted cycles**. Each valid cycle in lateral and DV matching views was scaled up/down as follows: the swing period was scaled up/down to $< t_{swing} >$, and the stride period to $(< t_{cycle} > - < t_{swing} >)$. This step included interpolation procedures.
7) **Selecting the best cycles in lateral and DV matching views**. For each lateral view cycle, the DV cycle best meeting the following requirement is selected: the greatest difference in length between the three leg segments should be minimal. The x and z cycle signals from the lateral view are completed with the y signal from the DV view, to obtain the reconstructed 3D signals.
8) **Averaging reconstructed 3D cycles**. This last step involved scaling up/down all best matching cycles using step 6 and averaging them.

The advantage of this technique is that the swing period is kept almost constant, whereas the stride period varies with the pace of the gait. Even if the foot signal is made continuous, this does not necessarily mean that other joint signals are also continuous. Indeed, some discontinuity may be observed, with a maximum amplitude of about $0.5\,cm$ between the beginning and end of the reconstructed 3D cycle. Unfortunately, it is difficult to overcome this problem.

TABLE I
DATA FOR THE 3D RECONSTRUCTION TECHNIQUE

Characteristics	Quail A	Quail B
No. of samples / signal	108	134
sample period in ms	3.7	4
No. of matched cycles	18	15
$< t_{cycle} >$ in s	0.40	0.59
$< t_{swing} >$ in s	0.14	0.22
average velocity in $m.s^{-1}$.	0.34	0.23

We used biological data recorded from two different quails for this study. The reconstructed data are summarized in table I. The precision of the technique is evaluated by determining the error rates for leg segments. We found that the error rate between reconstructions varied between 5% and 22%. Only reconstructions with error rates below 10% were used for subsequent kinematic analysis.

C. Qualitative description of the motion of a bird leg

1) Cyclograms and chronograms: Several different graphical representations can be used to analyze leg motion. These representations include 2D Cartesian trajectories (x, y), (x, z) and (y, z), which are known as cyclograms, chronograms of different coordinates, and chronograms for all articular angles. All these representations are complementary. Cyclograms provide a global view of leg motion, whereas chronograms provide precise information about local movement. Figures 6, 7 and 8 show cyclograms for right leg sagittal, DV and front views. The coordinate system is centered on the VC posterior point, VC_p, the axes of which are linked to the environment.

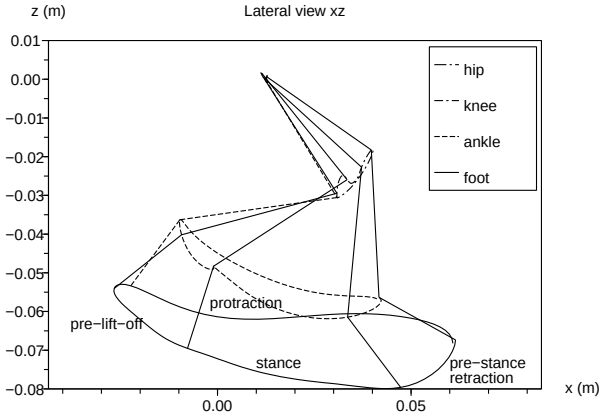

Fig. 6. Sagittal plane Cartesian trajectories (x, z) of the hip, knee, ankle and foot, defined in the coordinate system centered on the VC posterior point, VC_p, the axes of which are linked to the environment. Quail A right leg.

2) Walking cycle breakdown: The walking cycle can be broken down into four main phases: the stance phase, the pre-lift-off phase, the protraction phase and the pre-stance retraction phase.

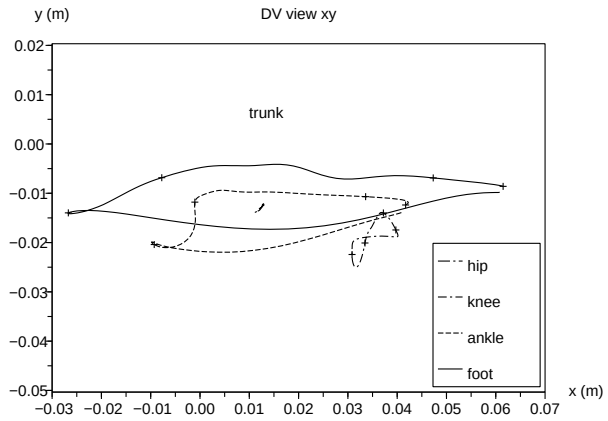

Fig. 7. Dorso-ventral plane Cartesian trajectories (x, y) of the hip, knee, ankle and foot, defined in the coordinate system centered on the VC posterior point, VC_p, the axes of which are linked to the environment. Quail A right leg.

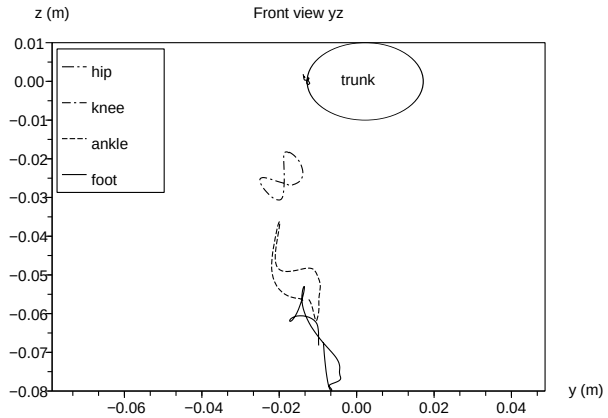

Fig. 8. Front plane Cartesian trajectories (y, z) of the hip, knee, ankle and foot, defined in the coordinate system centered on the VC posterior point, VC_p, the axes of which are linked to the environment. Quail A right leg.

- **Stance phase** $(11 - 47\%)$**.** The start of this phase coincides with footfall. At this moment in time, the tibiotarsus is almost part of a transverse vertical plane, with identical longitudinal coordinates for the knee and ankle (see fig. 9). The foot remains below the VC for most of this phase, whereas the knee and ankle shift laterally. The animal's motion is driven by the knee and ankle joints. The stance phase ends when the foot starts to lift off.
- **Pre-lift-off phase** $(47 - 66\%)$**.** This is the most complicated phase. It begins with the foot leaving the ground along the longitudinal axis, but with the toes remaining in contact with the ground and contributing to propulsion. The ankle and foot have the same longitudinal coordinate, implying that the tarsometatarsus belongs to the same transverse vertical plane. The foot then reaches its most backward position and the last toes leave the ground.
- **Protraction phase** $(66 - 100\%)$**.** The animal brings the foot back in the direction of motion. The foot goes forward until it is aligned below the ankle. Foot and ankle reach their apex at 71% of the cycle. The angle of the knee joint changes direction. During this phase, the entire leg is almost aligned into the same vertical plane. At the end, the ankle and foot pass through the same vertical plane.
- **Pre-stance retraction phase** $(0 - 11\%)$**.** This phase begins when the foot starts to descend. The knee extends to allow the foot to descend and touch the ground. This movement is assisted by horizontal rotation at the hip.

The period from the beginning of the support phase until two thirds of the way into the pre-lift-off phase, when the toes leave the ground, accounts for 60% of the total cycle. Figure 9 illustrates some particularly interesting moments in the cycle, where the leg reaches specific kinematic configurations. These configurations can be used for trajectory planning or position control.

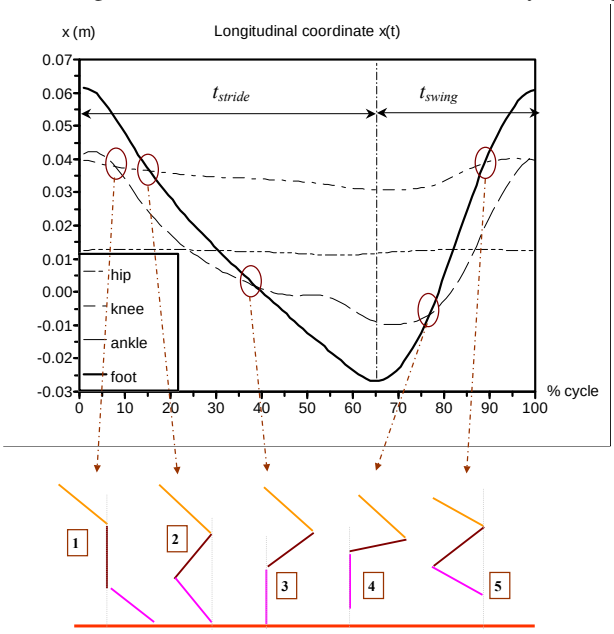

Fig. 9. Specific configurations of the leg during the walking cycle, with a duration of $< t_{cycle} >$. Projections of the hip, knee, ankle and foot joint onto the longitudinal axis of the direction of motion are shown.

This qualitative description of the 3D movement of the bird leg represents an innovation over previous studies on small biped animals. This analysis should enable robotics researchers to develop an understanding of this motion, facilitating the design of functional kinematic models.

III. Robotics Modeling

Our analysis of leg motion in this section focuses on the functional leg plane, and is based on calculations of angular velocity vectors. We aimed to check the number of active DOF at each joint and to determine the orientation of the rotation axes.

A. Functional leg plane

The first question to be addressed concerns whether all three segments belong to the same plane. To answer this question, we need to define a functional leg plane $(\mathcal{P})$ passing through the hip, knee and foot joints. Hip, knee and foot joint centers

- H, K and Ft - are never aligned. We therefore focused on hip and knee points because the femur drives motion of the whole leg. The foot belongs to the functional plane because it exerts effort on the ground.

We then estimated how close the ankle was to this plane throughout the cycle. This can be done in two ways. The first involves calculating the orthogonal distance $d_A^{\mathcal{P}}$ of the ankle A to the plane $(\mathcal{P})$. The second involves calculating the torsion angle α at the ankle between the plane defined by the femur and tibiotarsus, and the plane defined by the tibiotarsus and the tarsometatarsus.

Distance $d_A^{\mathcal{P}}$ is calculated as follows:

$$d_A^{\mathcal{P}} = \frac{\boldsymbol{n_1}.\boldsymbol{A}}{\|\boldsymbol{n_1}\|} = \frac{n_{1x}.x_A + n_{1y}.y_A + n_{1z}.z_A + d}{\sqrt{n_{1x}^2 + n_{1y}^2 + n_{1z}^2}} \quad (1)$$

where $\boldsymbol{n_1} = (n_{1x}, n_{1y}, n_{1z})$ is the normal to the functional plane defined by $\boldsymbol{n_1} = \boldsymbol{HK} \times \boldsymbol{HFt}$, and $d = -\boldsymbol{n_1}.H$.
The torsion angle α is given by:

$$\sin\alpha = sign[(\boldsymbol{n_1} \times \boldsymbol{n_2}).\boldsymbol{x_0}] \sqrt{(\boldsymbol{n_1} \times \boldsymbol{n_2}).(\boldsymbol{n_1} \times \boldsymbol{n_2})} \quad (2)$$

where $\boldsymbol{n_2} = \frac{\boldsymbol{HK} \times \boldsymbol{HA}}{\|\boldsymbol{HK} \times \boldsymbol{HA}\|}$.
As $\boldsymbol{n_1}$ and $\boldsymbol{n_2}$ are directed towards the body (right leg), a negative distance to the functional plane and a negative torsion angle imply that the ankle is turned outwards with respect to the functional plane. Distance and torsion angles

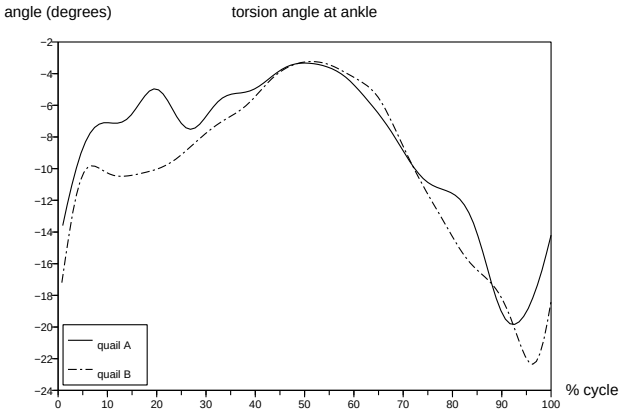

Fig. 10. Torsion angles at the ankle for quails A and B

remain negative and follow the same pattern throughout the cycle. Figure 10 shows variations in torsion angles for the two quails. Mean torsion angle is about -9° (range: -21° to -3°). These values suggest that the last segment, the tarsometatarsus, is inclined relative to the plane defined by the femur and the tibiotarsus. Given the negative sign of the torsion angle, the ankle is twisted outward, away from the body. During the stance phase, the torsion ankle and distance to the plane remain low, implying that the ankle is almost included in the functional plane. At the end of the pre-lift-off phase (60%), ankle torsion and distance suddenly begin to decrease, this decrease continuing until the start of landing, when they increase again. This abrupt change is related to the ankle and foot being freed from under the body at take-off, and to a kind of relaxation at the ankle resulting from joint elasticity.

B. Angular rotation kinematics

1) Notations: Starting from the hip, leg segments are numbered from 1 to 3. Body number is 0. s_1 denotes segment HK, s_2, segment KA, and s_3 segment AF. A coordinate system R_i is linked to each segment s_i, $i \in \{1, 2, 3\}$. $R_0 = (\boldsymbol{x_0}, \boldsymbol{y_0}, \boldsymbol{z_0})$ is the reference frame linked to the body, where $\boldsymbol{x_0}$ is the horizontal axis vector in the direction of motion, $\boldsymbol{z_0}$ is the vertical, and $\boldsymbol{y_0}$ is $\boldsymbol{z_0} \times \boldsymbol{x_0}$.
The instantaneous angular rotation vector of s_i relative to s_j is denoted by $\boldsymbol{\Omega_{i/j}}$. $\boldsymbol{\omega_{i/j}}$ designates the rotation angle variation vector of s_i relative to s_j.

$$\boldsymbol{\omega_{i/j}} = \boldsymbol{\Omega_{i/j}}.dt. \quad (3)$$

2) Kinematic equations: If we consider a first-order kinematic approximation, then the following three equations govern the motion of one segment relative to R_0, for $i \in \{1, 2, 3\}$:

$$\left\{\frac{\boldsymbol{ds_i}}{dt}\right\}_{R_0} = \left\{\frac{\boldsymbol{ds_i}}{dt}\right\}_{R_i} + \boldsymbol{\Omega_{i/0}} \times \boldsymbol{s_i} \quad (4)$$

As $\left\{\frac{\boldsymbol{ds_i}}{dt}\right\}_{R_i} = 0$, $\left\{\frac{\boldsymbol{ds_i}}{dt}\right\}_{R_0} = \left(\sum_{\boldsymbol{k=1}}^{\boldsymbol{i}} \boldsymbol{\Omega_{k/k-1}}\right) \times \boldsymbol{s_i}$.
Using $\boldsymbol{ds_i}$ variations, this system can be written as follows:

$$\boldsymbol{ds_i} = \left(\sum_{\boldsymbol{k=1}}^{\boldsymbol{i}} \boldsymbol{\omega_{k/k-1}}\right) \times \boldsymbol{s_i} \quad (5)$$

$d\boldsymbol{s_i}$ variations are obtained from reconstructed 3D biological data. They are related to the variation in $\boldsymbol{s_i}$ vectors between two consecutive images in the video sequence.
If we solve for rotation angle vectors $\boldsymbol{\omega_{k/k-1}}$, for $k \in \{1, 2, 3\}$, we obtain:

$$\sum_{k=1}^{i} \boldsymbol{\omega_{k/k-1}} = \alpha_i.\boldsymbol{u_i} + (\boldsymbol{u_{s_i}} \times \boldsymbol{ds_i})/s_i \quad (6)$$

with $\boldsymbol{u_i} = \boldsymbol{s_i}/s_i$, $s_i = |\boldsymbol{s_i}|$. Hence, $\forall(\alpha_i) \in \mathbb{R}^3$:

$$\begin{aligned}
\boldsymbol{\omega_{1/0}} &= \alpha_1.\boldsymbol{u_1} + (\boldsymbol{u_1} \times \boldsymbol{ds_1})/s_1 \\
\boldsymbol{\omega_{2/1}} &= \alpha_2.\boldsymbol{u_2} - \alpha_1.\boldsymbol{u_1} + (\boldsymbol{u_2} \times \boldsymbol{ds_2})/s_2 \\
&\quad -(\boldsymbol{u_1} \times \boldsymbol{ds_1})/s_1 \\
\boldsymbol{\omega_{3/2}} &= \alpha_3.\boldsymbol{u_3} - \alpha_2.\boldsymbol{u_2} + (\boldsymbol{u_3} \times \boldsymbol{ds_3})/s_3 \\
&\quad -(\boldsymbol{u_2} \times \boldsymbol{ds_2})/s_2
\end{aligned} \quad (7)$$

The choice of values (α_i) affects the kinematic joints appearing in the robotic model at each articulation. One goal is to minimize the number of active kinematic joints. If we consider the presence of a hinge joint along the first segment s_1 at the hip (see term $\alpha_1.\boldsymbol{u_{s_1}}$ in $\boldsymbol{\omega_{1/0}}$), then there is no point in having a hinge joint in the same direction at the knee K. We can therefore state that there is no hinge joint along s_1 at K:

$$\omega_{2/1}.\boldsymbol{u_1} = 0 \quad (8)$$

A hinge joint along s_2 is also more likely to occur at the ankle A than at the knee, as torsion is more likely to occur at the ankle than the knee, as borne out by our observations. So we have:

$$\omega_{2/1}.\boldsymbol{u_2} = 0 \quad (9)$$

A rotation about s_3 will not change the position of the foot and, given that toes feature some compliance, such a rotation would not need to be active, hence:

$$\omega_{3/2}.\boldsymbol{u_3} = 0 \tag{10}$$

Equations 8, 9, 10 and equation system 7 give:

$$\begin{aligned}
&\alpha_2.(\boldsymbol{u_2}.\boldsymbol{u_1}) - \alpha_1 + (\boldsymbol{u_2} \times \boldsymbol{ds_2}).\boldsymbol{u_1}/s_2 = 0\\
&\alpha_2 - \alpha_1.(\boldsymbol{u_1}.\boldsymbol{u_2}) - (\boldsymbol{u_1} \times \boldsymbol{ds_1}).\boldsymbol{u_2}/s_1 = 0\\
&\alpha_3 - \alpha_2.(\boldsymbol{u_2}.\boldsymbol{u_3}) - (\boldsymbol{u_2} \times \boldsymbol{ds_2}).\boldsymbol{u_3}/s_2 = 0
\end{aligned} \tag{11}$$

The solution for α_i is therefore:

$$\begin{aligned}
\alpha_1 &= \frac{\boldsymbol{u_1} \times \boldsymbol{u_2}}{\sin^2(\widehat{\boldsymbol{s_1}, \boldsymbol{s_2}})}.\left(\frac{\boldsymbol{ds_2}}{s_2} - (\boldsymbol{u_2}.\boldsymbol{u_1}).\frac{\boldsymbol{ds_1}}{s_1}\right)\\
\alpha_2 &= \frac{\boldsymbol{u_1} \times \boldsymbol{u_2}}{\sin^2(\widehat{\boldsymbol{s_1}, \boldsymbol{s_2}})}.\left((\boldsymbol{u_2}.\boldsymbol{u_1}).\frac{\boldsymbol{ds_2}}{s_2} - \frac{\boldsymbol{ds_1}}{s_1}\right)\\
\alpha_3 &= \alpha_2(\boldsymbol{u_2}.\boldsymbol{u_3}) - (\boldsymbol{u_2} \times \boldsymbol{u_3}).\frac{\boldsymbol{ds_2}}{s_2}
\end{aligned} \tag{12}$$

C. Model

Figures 11, 12 and 13 present the coordinates of the three angular vectors, $\omega_{1/0}$ in R_0, and $\omega_{2/1}$ and $\omega_{3/2}$ in R_{ft}, where frame R_{ft} designates the vector frame with axes of $\boldsymbol{x}_{ft} = \boldsymbol{u_2}$, $\boldsymbol{y}_{ft} = \boldsymbol{u_2} \times \boldsymbol{u_1}$, and $\boldsymbol{z}_{ft} = \boldsymbol{u_2} \times (\boldsymbol{u_2} \times \boldsymbol{u_1})$.

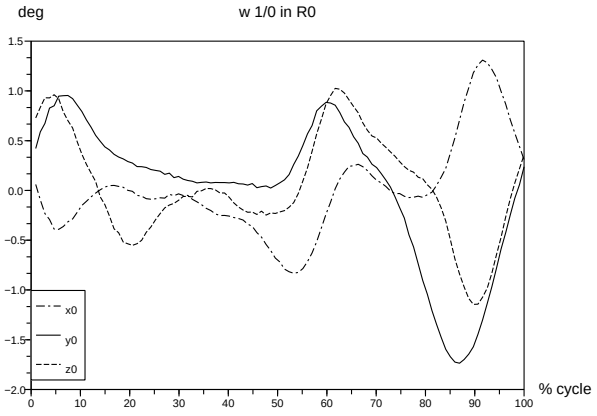

Fig. 11. Projections of angular vector $\omega_{1/0}$ in R_0. Quail A right leg.

As expected from calculation (§ III-B2), the knee joint has only one active degree of freedom, corresponding to rotation about the axis orthogonal to segments s_1 and s_2 (fig. 12). At the hip, rotation about $\boldsymbol{y_0}$ seems to have the largest amplitude and tends to be synchronized with rotation about $\boldsymbol{z_0}$ (fig. 11). At the ankle, rotation around the axis perpendicular to the first two segments has the largest amplitude, and this result is statistically significant (fig. 13). No apparent synchronization is observed among angular projections for the ankle.

1) Rough modeling: A rough kinematic model was generated based on three rotary actuators at the hip, one at the knee and one at the ankle [22] [23]. The ankle also has a passive hinge joint along the tibiotarsus, to take leg torsion into account. Figure 14 presents the kinematic scheme. The hip joint center has been broken down into three points O_1, O_2 and O_3, to facilitate understanding. The hip displays the classical

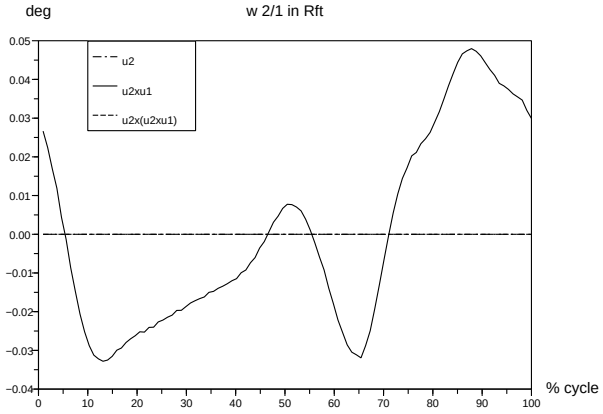

Fig. 12. Projections of angular vector $\omega_{2/1}$ in R_{ft}. Quail A right leg.

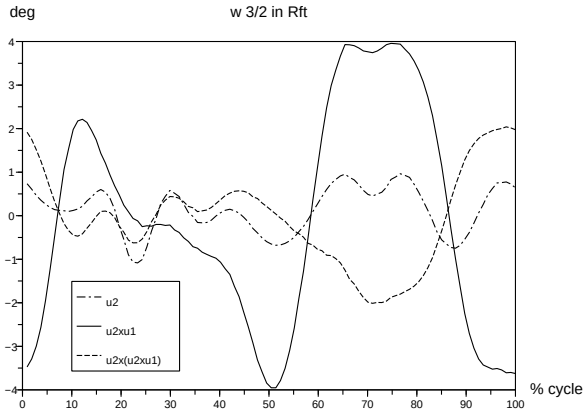

Fig. 13. Projections of angular vector $\omega_{3/2}$ in R_{ft}. Quail A right leg.

serial arrangement of three rotations with axes passing through the same point $H = O_1 = O_2 = O_3$. Starting from the body, the first rotation axis is vertical. The third rotation axis at the hip joint (O_3) is parallel to the active rotation axes of the knee and ankle. The second rotation at the hip (O_2) ensures rotation of the leg about a horizontal axis close to the direction of motion.

2) Precise modeling: The aim of precise modeling is to minimize the number of rotary actuators required to execute the leg trajectories used for walking. Underactuation is of prime importance in robotics, making it possible to achieve the same result with fewer mechanisms and motors. The orientation of the rotary joint axes is also important because it can help to achieve the desired trajectory with the minimum effort. The aim of precise modeling is to apply factor analysis to the calculated angular vectors. For bird legs, we focused on the hip and ankle.

From the angular vectors, we define points $\tilde{\Omega}^i_{1/0}$ for the hip at H, and points $\tilde{\Omega}^i_{3/2}$ for the ankle at A as follows:

$$\boldsymbol{H\tilde{\Omega}^i_{1/0}} = \boldsymbol{\Omega^i_{1/0}}|R_0 \tag{13}$$

$$\boldsymbol{A\tilde{\Omega}^i_{3/2}} = \boldsymbol{\Omega^i_{3/2}}|R_{ft} \tag{14}$$

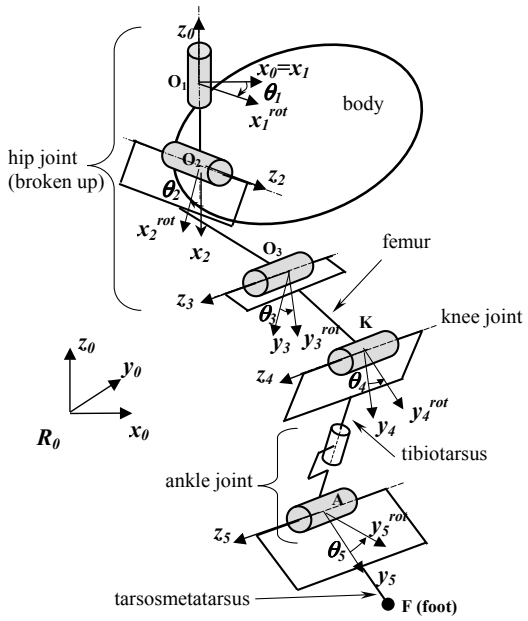

Fig. 14. Rough bird right leg kinematics with the direction of motion along $\boldsymbol{x_0}$. The hip joint can be broken down into three points: O_1, O_2 and O_3. Active rotations are shown in gray. There is a passive joint on the tibiotarsus.

We used Euclidean distance to identify the plane P_f that passes through the joint center and is closest to these points. We used factor analysis to obtain the three inertia axes of the set of points that pass through the center of the coordinate frame. Given a point C, a set of points $M_i(x_i, y_i, z_i)$, and their orthogonal projections $M_i^{\perp}$ onto the plane P_f passing through C, factor analysis finds the best plane P_f minimizing the criterion I:

$$I = \sum_i M_i M_i^{\perp 2} = \sum_i CM_i^2 - \sum_i CM_i^{\perp 2} \qquad (15)$$

Given that plane P_f is constrained to pass through center point C, minimizing I is equivalent to maximizing the inertia J on the plane P_f:

$$J = \sum_i CM_i^{\perp 2} \qquad (16)$$

If we denote by W (see eq. 17,18) the inertia matrix relative to the set of points to be considered, the direction of the factorial plane is given by the two eigenvectors of W with the highest eigenvalues. Each eigenvector $\boldsymbol{e_i}$ gives the direction of an inertia axis of the set of points. The maximal eigenvalue corresponds to the maximal inertia on the related inertia axis.

$$P = \begin{bmatrix} x_1 & y_1 & z_1 \\ \cdots & \cdots & \cdots \\ x_i & y_i & z_i \\ \cdots & \cdots & \cdots \\ x_n & y_n & z_n \end{bmatrix} \qquad (17)$$

$$W = P^T.P = \begin{bmatrix} \sum x_i^2 & \sum x_i.y_i & \sum x_i.z_i \\ \sum x_i.y_i & \sum y_i^2 & \sum y_i.z_i \\ \sum x_i.z_i & \sum y_i.z_i & \sum z_i^2 \end{bmatrix} \qquad (18)$$

TABLE II
FACTOR ANALYSIS RESULTS FOR THE HIP

Parameters	Quail A	Quail B
λ_1	0.025	0.036
λ_2	0.005	0.004
λ_3	0.003	0.002
$Q_1(P_f)$	0.77	0.87
$Q_2(P_f)$	0.91	0.96
$\boldsymbol{e_1}\|R_0$	$(-0.39, 0.77, 0.50)$	$(-0.34, 0.70, 0.63)$
$\boldsymbol{e_2}\|R_0$	$(0.79, 0.00, 0.61)$	$(0.60, 0.68, -0.45)$
$\boldsymbol{e_3}\|R_0$	$(-0.48, -0.63, 0.61)$	$(-0.74, 0.21, -0.64)$

TABLE III
FACTOR ANALYSIS RESULTS FOR THE ANKLE

Parameters	Quail A	Quail B
λ_1	0.240	0.144
λ_2	0.012	0.005
λ_3	0.004	0.003
$Q_1(P_f)$	0.93	0.95
$Q_2(P_f)$	0.98	0.98
$\boldsymbol{e_1}\|R_{ft}$	$(-0.08, -0.93, 0.35)$	$(-0.01, -0.92, 0.40)$
$\boldsymbol{e_2}\|R_{ft}$	$(0.67, 0.21, 0.71)$	$(0.99, -0.07, -0.14)$
$\boldsymbol{e_3}\|R_{ft}$	$(0.74, -0.30, -0.61)$	$(0.16, 0.39, 0.91)$

The quality factors $Q(P_f)$ of the approximation of the set of points by the factorial plane can be defined as follows:

$$Q_1(P_f) = \frac{\lambda_1}{\sum_{k=1}^{3} \lambda_k} \quad Q_2(P_f) = \frac{\lambda_1 + \lambda_2}{\sum_{k=1}^{3} \lambda_k} \qquad (19)$$

where λ_1 and λ_2 are the two largest eigenvalues of W.
Table II shows the results of factor analysis applied to the set of points $\tilde{\Omega}^i_{1/0}$ expressed in R_0 with center point H. Table III shows the results of factor analysis applied to the set of points $\tilde{\Omega}^i_{3/2}$ expressed in R_{ft} with center point A.

For both quails, the hip and ankle joints seem to have a main rotation axis, with a quality factor of about 0.82 for the hip and 0.94 for the ankle. This axis seems to be strongest for the ankle. Figures 15 and 16 present angle trajectories

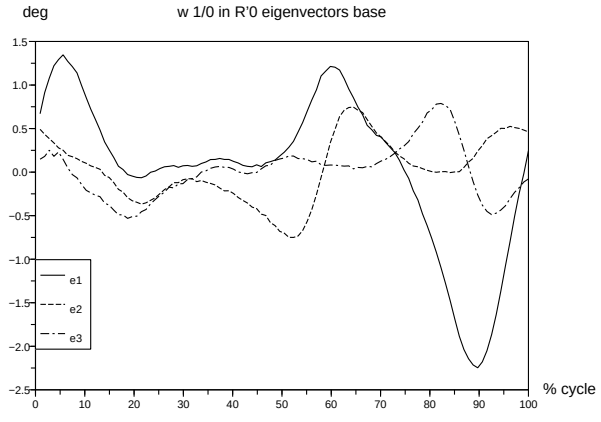

Fig. 15. Projections of angular vector $\omega_{1/0}$ on the eigenvector base from R_0. Quail A.

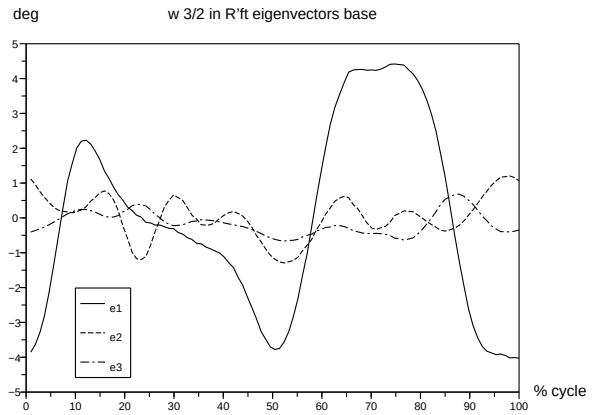

Fig. 16. Projections of angular vector $\omega_{3/2}$ on the eigenvector base from R_{ft}. Quail A.

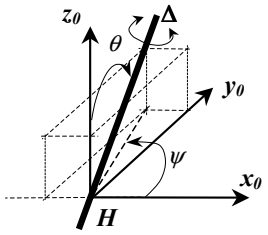

Fig. 17. Sideways backwards orientation of the hip main rotation axis Δ in frame R_0. $\boldsymbol{x_0}$ is the direction of motion.

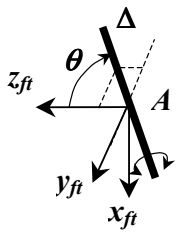

Fig. 18. Main rotation axis Δ at ankle in R_{ft}. $\boldsymbol{y_{ft}}$ is outwards from the functional plane. $\boldsymbol{x_{ft}}$ is the same direction as KA.

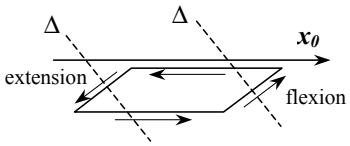

Fig. 19. Simplified diagram of foot trajectory in top view, to show the influence of an inclined rotation axis at the ankle.

TABLE IV
ROTATION AMPLITUDE INCREASE/DECREASE RATIOS AND MAIN AXIS ORIENTATION

	Hip		Ankle	
	Quail A	Quail B	Quail A	Quail B
% ↑ rot1	34	37	7	8
% ↓ rot2	-31	-37	-38	-62
% ↓ rot3	-38	-54	-34	-7
ψ (degrees)	117	116	-95	-91
θ (degrees)	60	51	69	66

in the coordinate frame defined by the eigenvectors obtained from factor analysis. The transformation of the frame, from its initial basis to an eigenvector basis, increases the amplitude of the rotation around the main axis and reduces the amplitude of rotation around the other two axes. Table IV shows the ratio of increase/decrease in joint angle amplitude between the initial and eigenvector frames. It also shows the orientation of the main rotation axes at the hip and ankle within the initial frame, using spherical angles ψ and θ. A similar orientation was obtained for both quails.

$$\psi = sign(\boldsymbol{e_1}.\boldsymbol{y}).\cos^{-1}(\boldsymbol{e_1}.\boldsymbol{x}/\sqrt{(\boldsymbol{e_1}.\boldsymbol{x})^2+(\boldsymbol{e_1}.\boldsymbol{y})^2}) \quad (20)$$

$$\theta = \cos^{-1}(\boldsymbol{e_1}.\boldsymbol{z}/\|\boldsymbol{e_1}\|) \quad (21)$$

The main rotation axis at the hip appears to be oriented sideways towards the body, and slightly backwards with mean spherical angles ψ of $116°$ and θ of $55°$ respectively. This first axis of hip rotation with respect to the body is consistent with the hip orientation used by the German designers of the Johnnie and LOLA humanoid robots [1], although they modeled their robot on a humanoid rather than a bird leg. In these robots, the first rotation axis was oriented at $15°$ to the vertical - a smaller inclination than observed for birds.
The main axis of rotation at the ankle is at a mean angle θ of $67°$ with respect to the y_{ft} axis. This axis is almost included in the yz plane.

The inclined orientations of the main rotation axes at the hip and ankle (see figures 17 and 18) make it possible to achieve the necessary foot trajectories, particularly during take-off and landing. In the landing phase, the foot must approach the longitudinal axis on the ground during its descent. In the take-off phase, the foot must move outwards from below the body whilst ascending. Figure 19 presents a simplified diagram of the trajectory of the foot in top view. Ankle extension about the main rotation axis Δ drives the foot away from the sagittal plane, whereas ankle flexion brings it back to the sagittal plane.
If we take the rotation with the second greatest amplitude into account, it has a quality factor greater than 0.9. The hip joint could therefore be underactuated with two degrees of freedom rather than three. However, the results for the second and third rotations are less significant, because they are related to smaller angles with respect to the maximum amplitude of rotation around the main axis. They are also subject to more measurement noise and error. Weighting of the factor analysis criterion J (eq. 16) could be introduced to minimize the influence of noise.

IV. DISCUSSION

Based on the measurement data obtained for quails, we suggest that, in the kinematic design of a bird-leg robot:

- The hip joint should be underactuated, using a main rotary joint with an axis oriented both to the side of and backwards of the body. Active or passive joints could be added, but these joints make a smaller contribution to motion than the main rotary joint. Further investigations of this point are required, with more precise measurements.
- The knee joint should have a single active degree of freedom - a rotary actuator with an axis perpendicular to the femur and the tibiotarsus.
- The ankle joint should be a major rotary joint turning around an inclined axis within the almost horizontal $(yz)_{ft}$ plane. For the right leg, this axis is oriented southwest to northeast for a north direction of motion. This makes it possible to twist the ankle outwards, away from the body. A passive joint could be added here but does not appear to be necessary, as compliance can be

transferred through the design of the toes, as explained below.

In this study, we took only forward displacements into account, because the quails were filmed in a longitudinal corridor. This raises questions about whether the leg kinematics design developed here is suitable for turns. The addition of a rotary actuator at the hip, such as a hinge joint along vertical axis z_0, may be required for turns, making it possible to change the direction of the entire leg to follow a new direction of motion. If rotations other than that about the main axis are to be taken into account (such as rotations at the hip for example), the related mechanisms may act in series or in parallel. If they act in series, it may be necessary to consider the order of rotations, and to adapt the orientation axes of the secondary rotations.

We used the measurements for only two quails here, because the data obtained for other quails were not exploitable, and because it is difficult to conduct biological experiments on a very large scale. So, do the results presented here apply to other birds? Complementary studies are required to address this question, but it seems likely that the main axis orientations at the hip and ankle are common to all kinds of birds, because all birds present the same leg configuration. The orientation angles may also depend on the ratios of leg segments.

In our future work, we intend to focus on the dynamics of bird locomotion. We are particularly interested in the influence of the orientation of these main axes on locomotion dynamics. Dynamic studies will also aim to determine the contribution of the toes to balance and propulsion. Based on biological observations of quails, we suggest that the robotic foot should have two or three toes, each driven by its own mechanism. There should be no mechanism for the foot itself. Each toe should feature an active rotary actuator along a horizontal axis, and one passive joint along the vertical axis. The passive joint should confer compliance on the leg when the foot is providing support. Toes could be actuated simultaneously.

Finally, this paper does not address the issue of control. Previous studies have made suggestions concerning how to control a redundant bird leg [24] by commanding the leg functional plane and commanding the foot within this plane. It has also been suggested that control could be broken down as a function of cycle phase, with different criteria used. Control techniques for bird redundant variations legs will be explored in future studies.

V. Conclusion

The results presented here were based on experiments conducted on walking quails. Biologists and roboticists cooperated to obtain a better understanding of the kinematics of the bird locomotor apparatus. This interaction between researchers from the two disciplines was initially difficult, but eventually proved highly fruitful. It will therefore be continued. The main achievement of this work is the design of a 3D reconstruction technique from two non-synchronized views (top and lateral). This led on to the kinematic modeling of a bird leg. Factor analysis made it possible to define the orientation of the main rotation axes at hip and ankle, leading to joint underactuation. The results of this study may facilitate the design of robotic legs taking their biological inspiration from the locomotor apparatus of birds.

Acknowledgment

We would like to thank the CNRS ROBEA (Robotics and Artificial Entities) programme for supporting the RoboCoq project [25] that allowed us to start our research on bird locomotion.

We also thank Pierre Blazevic for advice, and Paul Antoine Libourel for developing the semi-automatic software Loco version 4.1 in Matlab, dedicated to the extraction of 2D coordinates from quail X-ray video sequences.

References

[1] S. Lohmeier, T. Buschmann, H. Ulbrich, and F. Pfeiffer, "Modular joint design for performance enhanced humanoid robot LOLA," *IEEE Int. Conf. on Robotics and Automation*, pp. 88–93, 2006.

[2] K. Löffler, M. Gienger, and F. Pfeiffer, "Sensor and control design of a dynamically stable biped robot," *Proc. IEEE Int. Conference on Robotics and Automation*, pp. 484–490, 2003.

[3] Y. Kuroki, M. Fujita, T. Ishida, K. Nagasaka, and J. Yamaguchi, "A small biped entertainment robot exploring attractive applications," *Proc. IEEE Int. Conference on Robotics and Automation*, pp. 471–476, 2003.

[4] Y. Sakagami, R. Watanabe, C. Aoyama, S. Matsunaga, N. Higaki, and K. Fujimura, "The intelligent ASIMO: system overview and integration," *IEEE/RSJ Int. Conference on Intelligent Robot and System*, vol. 3, pp. 2478–2483, 2002.

[5] K. Kaneko, F. Kanehiro, S. Kajita, H. Hirukawa, T. Kawasaki, M. Hirata, K. Akachi, and T. Isozumi, "Humanoid robot HRP-2," *Proceedings of the IEEE International Conference on Rob. and Aut.*, pp. 1083–1090, 2004.

[6] A. Abourachid, "La marche des oiseaux – the walk of birds," *Thèse d'habilitation à diriger les recherches (in French), Paris XI University*, vol. 800, december 2004.

[7] ——, "Bipedal locomotion in birds: importance of functional parameters in terrestrial adaptation," *Anatidae Canadian Journal of Zoology*, vol. 78, pp. 1994–1998, 2000.

[8] M. A. Daley and A. A. Biewener, "Running over rough terrain reveals limb control for intrinsic stability," *Proc. of the Nat. Academy of Sciences of the U.S.A.*, vol. 103, no. 42, pp. 15 681–15 686, 2006.

[9] J. Rubenson, D. G. Lloyd, T. Besier, D. Heliams, and F. P.A., "Running in ostriches (Struthio camelus): three-dimensional joint alignment and joint kinematics," *The Journal of Experimental Biology*, vol. 210, pp. 2548–2562, 2007.

[10] J. Cracraft, "The functional morphology of the hind limb of the domestics pigeon," *Bulletin of the American Museum of Natural History*, vol. 144, pp. 175–265, 1971.

[11] M. Verstappen, P. Aerts, and R. Van Damme, "Terrestrial locomotion in the black-billed magpie: kinematics analysis of walking, running and out-of-phase hopping," *J. of Exp. Biol.*, vol. 203, pp. 2159–2170, 2000.

[12] S. M. Gatesy, "Guineafowl hind limb function. I: cineradiographic analysis and speed effects," *Journal of Morphology*, vol. 240, pp. 127–142, 1999.

[13] S. M. Reilly, "Locomotion in the quail (Coturnix coturnix japonica); the kinematics of walking and increasing speed," *Journal of morphology*, vol. 243, pp. 173–185, 2000.

[14] G. Nicolas, F. Multon, G. Berillon, and F. Marchal, "From bone to plausible bipedal locomotion using inverse kinematics," *Journal of Biomechanics*, vol. 40, no. 5, pp. 1048–1057, 2007.

[15] S. Kajita and K. Tani, "Experimental study of biped dynamic walking." *IEEE Control Systems*, vol. 16, no. 1, pp. 13–19, February 1996.

[16] J. Pratt, "Exploiting inherent robustness and natural dynamics in the control of bipedal walking robots," *PhD Thesis, Department of Electrical Engineering and Computer Science, Massachusetts Institute of Technology, Cambridge, Massachusetts*, 2000.

[17] G. Pratt, "Legged robots at mit: what's new since Raibert?" *IEEE Robotics and Automation Magazine*, vol. 3, no. 7, pp. 15–19, 2000.

[18] G. A. Pratt, "Low impedance walking robots," *Integ. and Comp. Biol.*, vol. 42, pp. 174–181, 2002.

[19] A. Witkin and Z. Popović, "Motion warping," *Proceedings of the 22nd annual conference on Computer graphics and interactive techniques*, pp. 105–108, 1995.

[20] G. Nicolas, F. Multon, G. Berillon, and F. Marchal, "Plausible locomotion for bipedal creatures using motion warping and inverse kinematics," *CGI 2006, Lecture Notes in Computer Science 4035*, pp. 586–593, 2006.
[21] A. Abourachid, "Comparison of kinematic parameters of terrestrial locomotion in cursorial (ratites) swimming (ducks) and striding birds (quail and guinea fowl)," *Comp Biochem Physiol A Mol Integr Physiol.*, vol. 131(1), pp. 113–119, 2001.
[22] L. Mederreg, V. Hugel, P. Blazevic, and A. Abourachid, "Modelling and design of a bird-like robot," in *Proceedings of the 6th International Conference on Climbing and Walking Robots (CLAWAR)*, Catane, Italy, Sept. 2003, pp. 761–768.
[23] L. Mederreg, V. Hugel, A. Abourachid, P. Blazevic, and R. Hackert, "Bird-leg kinematics and analysis," in *Proceedings of International Computer System and Information Technology (ICSIT)*, Algiers, Algeria, July 2005, pp. 123–127.
[24] L. Mederreg, V. Hugel, A. Abourachid, and R. Hackert, "Finding adequate optimization criteria to solve inverse kinematics of redundant bird leg mechanism," in *Proceedings of the 8th International Conference on Climbing and Walking Robots (CLAWAR)*, London, UK, Sept. 2005, pp. 319–362.
[25] V. Hugel, A. Abourachid, L. Mederreg, H. Gioanni, and P. Blazevic, "the Robocoq project : Modelling and design of a bird-like robot equipped with stabilized vision," in *Long Abstract Proceedings of the Second International Symposium on Adaptive Motion of Animals and Machines (AMAM)*, Kyoto, Japan, March 2003, p. 44.